AMERICAN SOCIETY of
GENE & CELL
THERAPY

Tat-haFGF₁₄₋₁₅₄ Upregulates ADAM10 to Attenuate the Alzheimer Phenotype of APP/PS1 Mice through the PI3K-CREB-IRE1α/XBP1 Pathway

Tian Meng,[1] Qin Cao,[1] Peng Lei,[3] Ashley I. Bush,[3] Qi Xiang,[1,2] Zhijian Su,[1,2] Xiang He,[1] Jack T. Rogers,[4] Ing-Ming Chiu,[5] Qihao Zhang,[1,2] and Yadong Huang[1,2]

[1]Guangdong Provincial Key Laboratory of Bioengineering Medicine, Jinan University, Guangzhou 510632, China; [2]Cell Biology Department and National Engineering Research Center of Genetic Medicine, Jinan University, Guangzhou 510632, China; [3]Oxidation Biology Unit, Florey Institute of Neuroscience and Mental Health, The University of Melbourne, Parkville, VIC 3010, Australia; [4]Neurochemistry Laboratory, Department of Psychiatry, Massachusetts General Hospital and Harvard Medical School, Charlestown, MA 02114, USA; [5]Institute of Cellular and System Medicine, National Health Research Institutes, Miaoli 35053, Taiwan

Acid fibroblast growth factor (aFGF) has shown neuroprotection in Alzheimer's disease (AD) models in previous studies, yet its mechanism is still uncertain. Here we report that the efficacy of Tat-haFGF₁₄₋₁₅₄ is markedly increased when loaded cationic liposomes for intranasal delivery are intranasally administered to APP/PS1 mice. Our results demonstrated that liposomal Tat-haFGF₁₄₋₁₅₄ treatment significantly ameliorated behavioral deficits, relieved brain Aβ burden, and increased the expression and activity of disintegrin and metalloproteinase domain-containing protein 10 (ADAM10) in the brain. Tat-haFGF₁₄₋₁₅₄ antagonized Aβ₁₋₄₂-induced cell death and structural damage in rat primary neurons in an ADAM10-dependent manner, which, in turn, was promoted by the activation of XBP1 splicing and modulated by the PI3K-CREB pathway. Both knockdown of ADAM10 and inhibition of PI3K (LY294002) negated Tat-haFGF₁₄₋₁₅₄ rescue. Thus, Tat-haFGF₁₄₋₁₅₄ activates the IRE1α/XBP1 pathway of the unfolded protein response (UPR) against the endoplasmic reticulum (ER) stress induced by Aβ, and, subsequently, the nuclear translocation of spliced XBP1 (XBP1s) promotes transcription of ADAM10. These results highlight the important role of ADAM10 and its activation through the PI3K-CREB-IRE1α/XBP1 pathway as a key factor in the mechanism of neuroprotection for Tat-haFGF₁₄₋₁₅₄.

INTRODUCTION

Alzheimer's disease (AD) is the main cause of progressive dementia. The senile plaques and neurofibrillary tangles (NFTs), which are composed of self-polymerized amyloid-β peptide (Aβ) and hyperphosphorylated tau proteins, respectively, are the two major pathological hallmarks in brains of AD.[1] Pathogenic Aβ aggregates initiate a cascade of molecular events that foster widespread neurodegeneration,[2] although the exact pathogenesis from Aβ aggregation to neurodegeneration is not clear. Aβ originates from proteolysis of the amyloid precursor protein (APP) by the sequential enzymatic actions of beta-site amyloid precursor protein-cleaving enzyme 1 (BACE1), β-secretase, and γ-secretase, a protein complex with pre-

senilin 1 (PS1) at its catalytic core.[3] α-secretase ADAM10 conversely cleaves APP within the eventual Aβ sequence to preclude Aβ generation, and it yields the N-terminal protein of APP (soluble APP-α [sAPPα]). sAPPα decreases Aβ generation by directly associating with BACE1, and so it may be a potential agent to ameliorate imbalances in APP processing.[4,5] Overexpression of ADAM10 markedly reduces Aβ plaque load and soluble Aβ, restoring learning deficits in a double-transgenic Alzheimer mouse model.[6] ADAM10 also plays a critical role in regulating functional membrane proteins at the synapse.[7]

Neurotrophins (neurotrophic factors [NTFs]) are important in the development, differentiation, and regeneration of brain neurons. In recent years, some neurotrophins, such as nerve growth factor (NGF) and brain-derived neurotrophic factor (BDNF), were explored as candidate therapeutics for AD.[8,9] Human acidic fibroblast growth factor (haFGF) has neuroprotective functions similar to NTFs'. Exogenous administration of haFGF has been shown to prevent degeneration and apoptosis of neurons in epileptic seizure.[10,11] haFGF is involved in the regulation of synaptic plasticity, processes attributed to learning and memory through improving cholinergic nerve functions.[12] haFGF showed a neuroprotective effect against brain injury resulting from focal ischemia-reperfusion in rats,[13,14] and it repaired human spinal cord injury in a clinical trial.[15,16] It is reported that the concentration of acid fibroblast growth factor (aFGF) is increased in the serum and cerebrospinal fluid of patients with AD.[17]

CrossMark

However, due to its large molecular size of 17 kDa, the 154-amino acid protein haFGF is unable to freely pass through biological membranes and the blood-brain barrier (BBB). This limits its application in brain disorders. Novel strategies were used to address this bottleneck problem, such as fusing the target protein with Tat-PTD[18] and utilizing intranasal delivery.[19,20] Our previous study showed that modified protein Tat-haFGF$_{14-154}$ could penetrate the BBB and was distributed in hippocampus and cortex via intravenous injection.[18] Following intranasal administration, the distribution of Tat-haFGF$_{14-154}$ was observed at 15 min in the brains of rats.[21] Tat-PTD could increase the concentration of haFGF in brain, and Tat-haFGF$_{14-154}$ improved cognition and reduced Aβ plaques more significantly than haFGF$_{14-154}$ in senescence-accelerated mouse prone-8 (SAMP8) and APP/PS1 mice.[22,23] Meanwhile, liposomes have gained increasing attention as a promising strategy for brain-targeted drug delivery due to their large delivery capabilities, capacity for surface decoration,[24] low toxicity, and biocompatibility with biodegradability.[25] Studies have shown that liposomes easily cross the BBB through absorptive mediated transcytosis.[26]

In the current study, Tat-haFGF$_{14-154}$ was encapsulated with cationic liposomes, and it was delivered to the APP/PS1 double-transgenic mouse model for AD via intranasal administration to investigate neuroprotection. The molecular mechanism related to neuroprotection of Tat-haFGF$_{14-154}$ was also explored in primary cortical neurons of rats injured by Aβ$_{1-42}$. Results demonstrated that Tat-haFGF$_{14-154}$ ameliorated the AD phenotype by increasing ADAM10 expression at the transcriptional level through the PI3K-CREB-IRE1α/XBP1 pathway, thereby enhancing ADAM10 enzyme activity.

RESULTS

Tat-haFGF$_{14-154}$-Loaded Cationic Liposomes Attenuate Behavioral Deficits in APP/PS1 Mice

Tat-haFGF$_{14-154}$-loaded cationic liposomes were produced and optimized in a series of experiments. The highest entrapment efficiency was achieved with a 1:2 ratio of Tat-haFGF$_{14-154}$ and liposomes incubated at 25°C or 30°C for 0.5 hr (∼97%; Figure S1A). These conditions did not alter the electrophoretic mobility profile of Tat-haFGF$_{14-154}$ on SDS-PAGE (Figure S1B). After a single intranasal administration, aFGF was detected in the olfactory bulb (OB) and entorhinal cortex (EC) of 7-month-old C57BL/6 mice (Figure S1C). Both Tat-haFGF$_{14-154}$ (600 μg/kg, T600) and Tat-haFGF$_{14-154}$-loaded cationic liposomes (600 μg/kg, L + T600) significantly enhanced the levels of aFGF in the OB (p < 0.05 for T600, p < 0.01 for L + T600 versus vehicle; Figure S1D); only L + T600 enhanced the levels of aFGF significantly in the EC (p < 0.01 versus vehicle; Figure S1E). Intranasal treatment of Tat-haFGF$_{14-154}$-loaded cationic liposomes demonstrated a higher efficiency for the delivery of aFGF compared with Tat-haFGF$_{14-154}$ alone, as evidenced by the significantly elevated levels of aFGF in the EC (p < 0.01 for L + T600 versus T600; Figure S1E).

Tat-haFGF$_{14-154}$-loaded cationic liposomes were delivered intranasally to 7-month-old APP/PS1 mice every 2 days for 6 weeks, followed by a Morris water maze (MWM) test in the fifth week and nest construction (NC) and open field (OF) tests in the sixth week (Figure 1A). The MWM was used to observe cognitive behavior of APP/PS1 mice. Representative movement tracks of mice on day 5 in the place navigation component of the MWM are shown in Figure 1B. Both T600 and L + T600 significantly decreased the escape latency compared with vehicle (p < 0.001 for T600 and L + T600; Figure 1C). Mice treated with L + T600 exhibited a shorter escape latency compared to those treated with T600 (p < 0.01; Figure 1C) during the 6 days of testing. T600 and L + T600 also decreased the path length in APP/PS1 mice compared with vehicle during the 6 days of tests (p < 0.001 for T600 and L + T600; Figure 1D). L + T600 exhibited a notably shorter path length from day 3 (p < 0.05 on day 3, p < 0.01 on days 4 and 5; Figure 1E), whereas this was only evident with T600 on day 5 (p < 0.05; Figure 1E) compared with vehicle. After finishing the navigation test on day 5, a spatial probe test was conducted 24 hr later. Movement tracks, the incidence of crossing the removed-platform area, and percentage of time spent in target quadrant were recorded (Figures 1F–1H). L + T600 significantly increased the incidence of crossing the removed-platform area (p < 0.01; Figure 1G) and time spent in the target quadrant (p < 0.01; Figure 1H) compared with vehicle. There were no differences in the swimming speed of mice among all groups in the place navigation and spatial probe tests (Figure S2A). These results indicate that Tat-haFGF$_{14-154}$-loaded cationic liposomes significantly attenuated cognitive behavior deficits and that the liposome Tat-haFGF$_{14-154}$ preparation was more potent than Tat-haFGF$_{14-154}$ alone.

Next, non-cognitive behaviors were examined in APP/PS1 mice, including NC and OF tests in the sixth week after intranasal administration. Body weights of mice had no significant change in the whole experimental period (Figure S2B). It is reported that APP/PS1 mice fail to construct nests[27] and display an increased locomotor activity compared with wild-type mice.[28,29] The nesting scores of the PS1/APP mice improved significantly with both T600 and L + T600 treatments (p < 0.01 for T600, p < 0.01 for L + T600; Figures S3A and S3B). In the OF test, L + T600 significantly decreased time spent (p < 0.05; Figure S3C) and crossing times (p < 0.01; Figure S3D) in the central area, and it shortened the total distance of movement (p < 0.01; Figure S3E) compared with vehicle. L + T600 treatment was significantly more effective than T600 in the OF test (p < 0.05 in Figure S3C and p < 0.01 in Figure S3E).

Tat-haFGF$_{14-154}$-Loaded Cationic Liposomes Reduce Brain Aβ Burden in APP/PS1 Mice

Overload of Aβ plaque is the major pathology in the brain of APP/PS1 mice. Aβ plaques were assessed by immunohistochemisty in the cortex and hippocampus (cornu ammonis 1 [CA1] is illustrated in Figure 2A). The percentage area and number of Aβ plaques in coronal sections were calculated. L + T600 treatment reduced the area (p < 0.01; Figure 2B) and the number (p < 0.001; Figure 2C) of Aβ plaques compared with vehicle. Although T600 decreased the Aβ plaque number (p < 0.05; Figure 2C), it did not significantly change
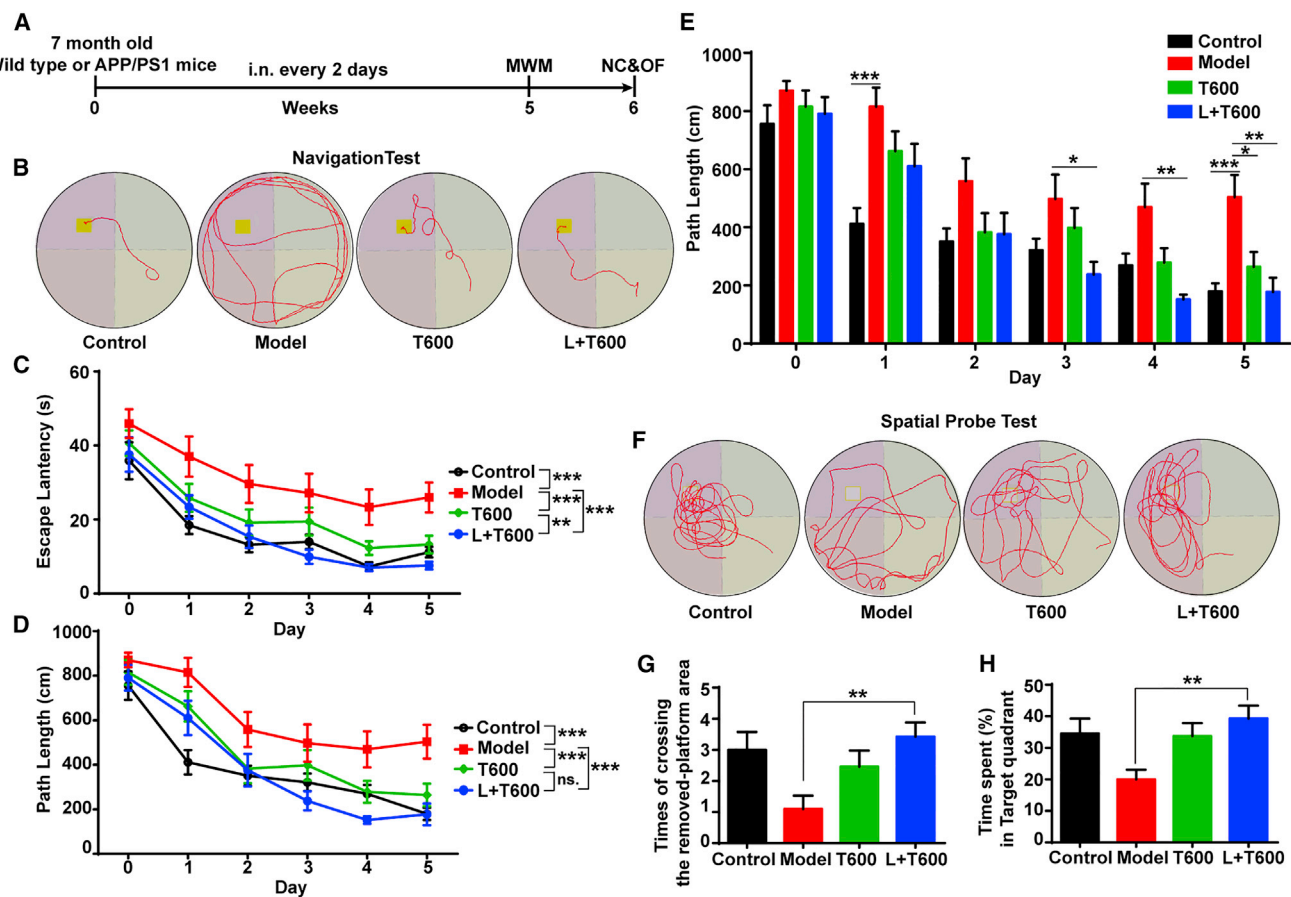
Figure 1. Tat-haFGF$_{14-154}$-Loaded Cationic Liposomes Attenuated Cognitive Behavioral Deficits in APP/PS1 Mice

(A) Schematic of the protocol followed for the experiments. Aliquots of 0.9% saline (vehicle), Tat-haFGF$_{14-154}$ (600 µg/kg, T600), and Tat-haFGF$_{14-154}$-loaded cationic liposomes (600 µg/kg, L + T600) were delivered intranasally to 7-month-old APP/PS1 mice every 2 days for 6 weeks (n = 8). MWM was conducted in the fifth week, and nest construction (NC) and OF tests were in the sixth week. (B–E) Navigation test in MWM. Representative movement tracks of mice on day 5 (B), escape latencies (C), and path length (D and E) over the 5 days are shown. (F–H) Following the completion of the navigation test, a spatial probe test was conducted 24 hr later. Representative movement tracks (F), percentage of time mice spent in the target quadrant (G), and times of crossing the removed-platform area (H) were assessed. All values are presented as means ± SEM (n = 8; *p < 0.05, **p < 0.01, and ***p < 0.001, two-way ANOVA with Bonferroni post hoc test for C–E, one-way ANOVA with Bonferroni's post hoc test for G and H). i.n., intranasal administration; MWM, Morris water maze; OF, open field; ns., no significance.

the percentage of the Aβ plaque area. To further confirm these results, tissue homogenates from cortex and hippocampus were used to detect Aβ by western blotting (Figures 2D–2F). L + T600 reduced Aβ levels both in cortex (p < 0.05; Figure 2E) and hippocampus (p < 0.01; Figure 2F) compared with vehicle. These results indicate that Tat-haFGF$_{14-154}$-loaded cationic liposomes decreased Aβ burden in the brain of APP/PS1 mice and were more effective than Tat-haFGF$_{14-154}$ alone.

Tat-haFGF$_{14-154}$-Loaded Cationic Liposomes Enhance Expression and Activity of ADAM10 in the Brain of APP/PS1 Mice

To determine whether the reduction of Aβ loading could be due to a change in APP-processing modulation, the expression of APP and its processing proteins (ADAM10, BACE1, and PS1) in cortex and hippocampus was measured by western blotting (Figure 3A). The expression of ADAM10 (p < 0.01 in cortex, Figure 3B; p < 0.05 in hippocampus, Figure 3F), but not full-length APP (FL-APP, Figures 3C and 3G) or BACE1 (Figures 3D and 3H), was enhanced significantly by L + T600 both in cortex and hippocampus compared with vehicle. L + T600 enhanced the expression of PS1 (p < 0.05; Figure 3I) in hippocampus, but not in cortex. T600 had no influence on the expression of the above proteins (Figures 3B–3I). Enzyme activities of ADAM10 and BACE1, two major secretases in APP processing,[30] were assayed from hippocampus homogenates of APP/PS1 mice. The activity of ADAM10 (p < 0.05; Figure 3J), but not BACE1 (Figure 3K), was increased by L + T600 compared with vehicle. These results revealed that the reduction of Aβ loading in the brain of APP/PS1 mice treated with Tat-haFGF$_{14-154}$-loaded cationic liposomes could be due to the enhancement of ADAM10 in expression and activity.
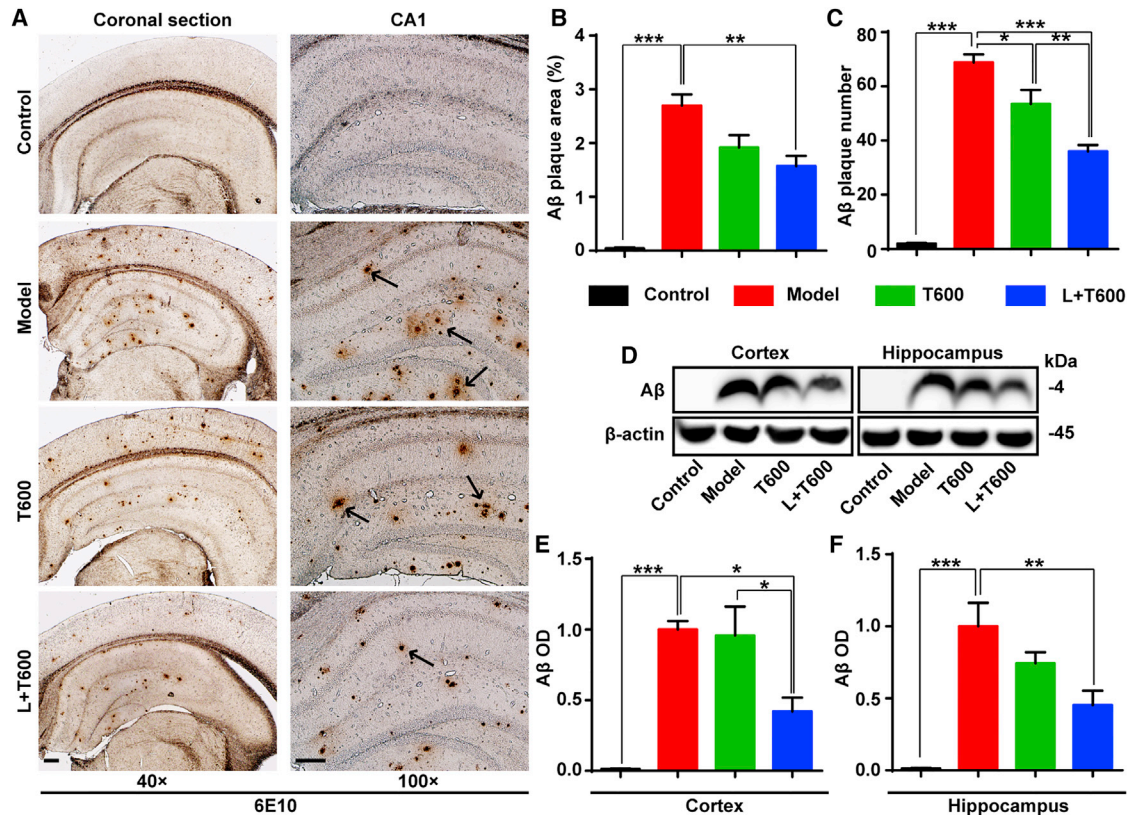
Figure 2. Tat-haFGF$_{14-154}$-Loaded Cationic Liposomes Reduced Aβ Loading in the Brain of APP/PS1 Mice

(A) Representative images of Aβ plaques in coronal section and CA1 area of brain (scale bar, 80 μm). The black arrows show Aβ plaque. (B and C) Percentage of Aβ plaque area (B) and plaque number (C) in coronal sections were analyzed by Image-Pro plus (n = 8). (D–F) Representative immunoblots (D) and quantification of Aβ expression in cortex (E) and hippocampus (F) (n = 6). All values are presented as means ± SEM (*p < 0.05, **p < 0.01, and ***p < 0.001, one-way ANOVA with Bonferroni post hoc test). OD, relative optical density.

Tat-haFGF$_{14-154}$ Protects Neurons from Damage Induced by Aβ_{1-42} In Vitro

Primary cortical neurons at 5 days in vitro (DIV) were incubated with Aβ_{1-42} oligomers for 48 hr at 37°C. Aβ_{1-42} (1.5 μM) suppressed the viability of primary cortical neurons to 69.7% ± 1.4% (p < 0.001; Figure 4A), and apoptotic bodies/karyopyknosis affected 34.3% ± 4.4% of the cells (p < 0.001; Figures 4B and 4C), compared to control cells. Neurons at 5 DIV were pre-treated with Tat-haFGF$_{14-154}$ (60 ng/mL [T60], 300 ng/mL [T300], and 1,500 ng/mL [T1500]) for 2 hr at 37°C. Aβ was added to the culture medium with continuous Tat-haFGF$_{14-154}$ treatment for 48 hr. Upon treatment with Tat-haFGF$_{14-154}$, cell viability was significantly increased to 84.5% ± 3.0% (T60 + Aβ), 90.4% ± 3.5% (T300 + Aβ), and 97.4% ± 1.9% (T1500 + Aβ), compared with untreated cells (p < 0.01 for T60 + Aβ, p < 0.001 for T300 + Aβ, and p < 0.001 for T1500 + Aβ; Figure 4A). Nuclear staining (Hoechst 33342) revealed that the prevalence of karyopyknosis or apoptotic body formation induced by Aβ_{1-42} was diminished by Tat-haFGF$_{14-154}$ in a concentration-dependent manner (p < 0.05 for T60 + Aβ, p < 0.001 for T300 + Aβ, and p < 0.001 for T1500 + Aβ; Figures 4B and 4C). Morphologic structure of neurons was observed by scanning electron microscopy

(Figure 4D). As showed in micrographs, somata were flat and fractured and neurites were fragmented in neurons injured by Aβ. This damaged appearance was reversed by the treatment with Tat-haFGF$_{14-154}$ in a concentration-dependent manner.

To further estimate the degree of injury in neurites, two synaptic markers, synaptophysin (SYN) and growth-associated protein 43 (GAP43), were assessed by immunofluorescence and western blotting in primary cortical neurons (Figure S4). Both assays revealed that levels of SYN and GAP43 were suppressed by Aβ (p < 0.05 or p < 0.01) but that this was successfully rescued by the Tat-haFGF$_{14-154}$ treatment (p < 0.01 or p < 0.001). Levels of SYN and GAP43 were also assessed in the brains of APP/PS1 mice by immunohistochemistry and western blotting (Figure S5). The immunohistochemistry detected SYN and GAP43 located in different regions of hippocampus in wild-type healthy control mice (Figure S5A). SYN was mainly located in the dentate gyrus (DG) area, whereas GAP43 was mainly located in CA1 area. Therefore, the effects of treatment on the levels of SYN in the DG area (Figures S5B and S5D) and GAP43 in the CA1 area (Figures S5C and S5E) were assessed. L + T600 increased the levels of SYN in the DG area (p < 0.01; Figure S5D) and GAP43 in the CA1
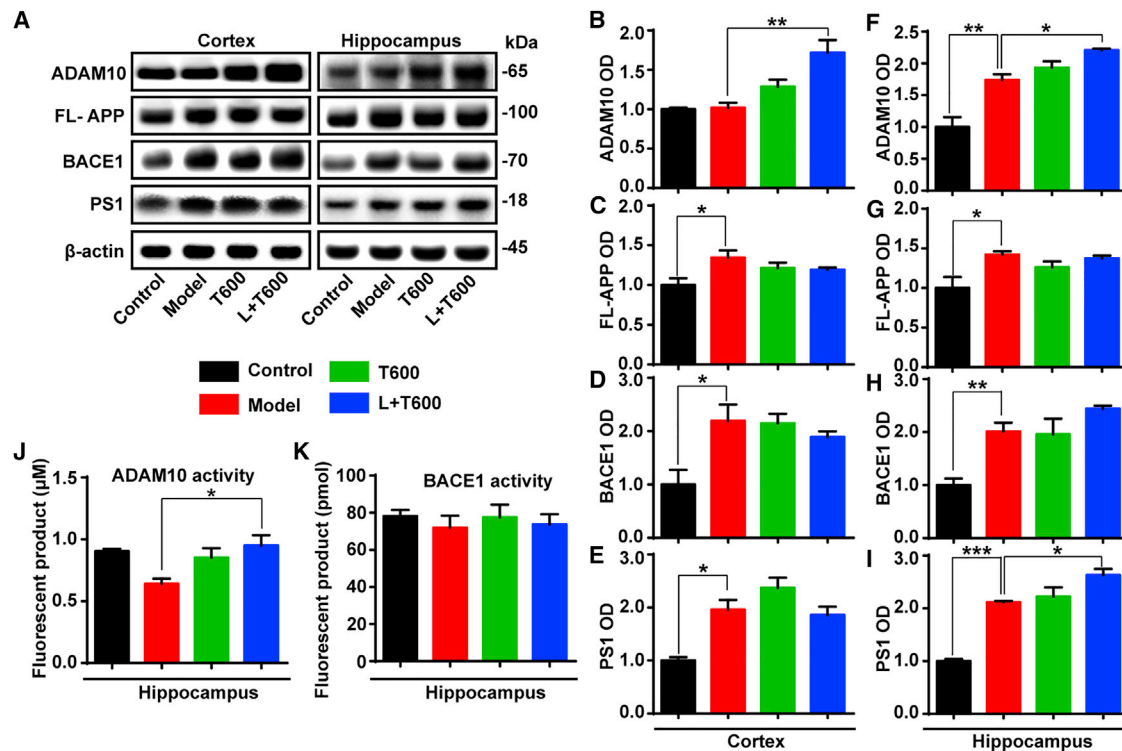
Figure 3. Tat-haFGF$_{14-154}$-Loaded Cationic Liposomes Enhanced ADAM10 Expression and Activity in the Brain of APP/PS1 Mice

(A–I) Representative immunoblots (A) and quantification expression of APP-processing proteins in cortex (B–E) and hippocampus (F–I) of APP/PS1 mice. APP-processing proteins, including FL-APP, ADAM10, BACE1, and PS1, were assayed by western blotting. (J and K) ADAM10 activity (J) and BACE1 activity (K) in homogenate of hippocampus were measured by an enzymatic cleavage assays. All values are presented as means ± SEM (n = 6; *p < 0.05 and **p < 0.01, one-way ANOVA with Bonferroni post hoc test). FL-APP, full-length APP; OD, relative optical density.

area (p < 0.001; Figure S5E) compared with vehicle. Western blotting for SYN and GAP43 (Figures S5F–S5J) validated these conclusions. Although there were no significant changes of SYN and GAP43 levels in the cortex (Figures S5G and S5H), L + T600 enhanced the levels of SYN (p < 0.05; Figure S5I) and GAP43 (p < 0.05; Figure S5J) in the hippocampus compared with vehicle. T600 did not change the expression levels of SYN and GAP43 in the cortex and hippocampus (Figures S5D–S5J).

Neuroprotection of Tat-haFGF$_{14-154}$ Is Abolished by Knockdown of ADAM10

The expression of ADAM10, both mRNA and protein, in primary neurons was significantly enhanced by Tat-haFGF$_{14-154}$ (p < 0.05 for T300 + Aβ and p < 0.01 for T1500 + Aβ in mRNA level, Figure 5A; p < 0.01 for T1500 + Aβ in protein level, Figure 5C). ADAM10 activity in primary neurons was also elevated by Tat-haFGF$_{14-154}$ (p < 0.01 for T300 + Aβ and p < 0.001 for T1500 + Aβ; Figure 5D). The enhancement of ADAM10 in expression and enzyme activity both in vivo (Figure 3) and in vitro indicated that ADAM10 might be a key target for Tat-haFGF$_{14-154}$ to protect neurons from injury in AD models.

To validate this possibility, small interfering RNA (siRNA) targeting of ADAM10 was tested in rat primary cortical neurons at 5 DIV.

Knockdown was confirmed over 24–72 hr by qRT-PCR and western blotting, and it was not affected by Aβ treatment for 48 hr (Figure S6). Normal neurons (T1500 + Aβ) or ADAM10-knockdown (KD) neurons (KD + T1500 + Aβ) were incubated with Tat-haFGF$_{14-154}$ and Aβ$_{1-42}$ as described above. The siRNA knockdown blocked the elevation of ADAM10 induced by Tat-haFGF$_{14-154}$ (p < 0.01 for Aβ and p < 0.001 for KD + T1500 + Aβ; Figure 6B), and it significantly impaired the ability of T1500 to rescue Aβ toxicity (p < 0.01; Figure 6C) and Aβ damage to soma and neurites (Figure 6D).

Tat-haFGF$_{14-154}$ Regulates ADAM10 via the PI3K-CREB-IRE1α/XBP1 Pathway

X-box-binding protein 1 (XBP1) is one of the transcription factors of ADAM10, and it is also linked with the unfolded protein response (UPR). XBP1 suppression has been observed in AD brain tissue.[31] Spliced XBP1 protein (XBP1s) is the activated form of XBP1, and the ratio of XBP1s and unspliced XBP1 (XBP1u) reflects the activity of XBP1. After nuclear translocation, XBP1s binds to its binding site on the ADAM10 mRNA promoter and promotes transcription.[32] XBP1s/XBP1u was significantly increased by L + T600 in the cortex (p < 0.05; Figure S7B), by T600 and L + T600 in the hippocampus (p < 0.01 for T600 and p < 0.05 for L + T600; Figure S7C) compared to vehicle-treated mice, indicating that XBP1 was activated by
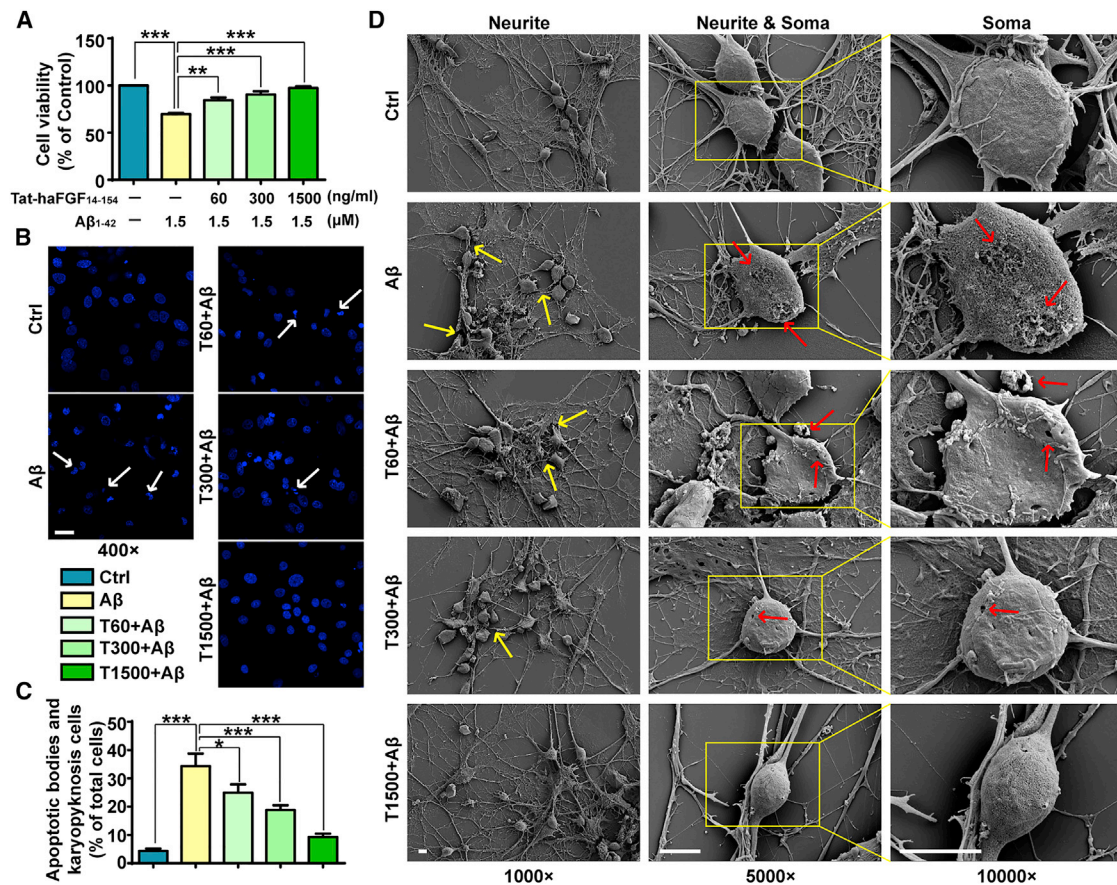
Figure 4. Tat-haFGF$_{14-154}$ Protected Neurons from Damage Induced by Aβ_{1-42}

Primary cortical neurons were isolated from brains of newborn SD rats. DIV5 (5 days in vitro) neurons were pre-treated with Tat-haFGF$_{14-154}$ (60, 300, and 1,500 ng/mL) for 2 hr at 37°C, and 1.5 μM Aβ_{1-42} was added into the culture medium with continuous Tat-haFGF$_{14-154}$ treatment for 48 hr. (A) Cell viability was detected by MTT assay (n = 6). (B) Representative immunofluorescence images of Hoechst 33342 staining (scale bar, 20 μm). The white arrows show apoptotic bodies or karyopyknosis cells. (C) The percentage of cells exhibiting apoptotic bodies or karyopyknosis (blue) was calculated (n = 20). (D) Representative images of cell surface structure were captured by scanning electron microscope (scale bar, 4 μm). The yellow arrows show fractured neurites or axons, and the red arrows show desiccated or shrinking somata. Values are presented as means ± SEM (*p < 0.05, **p < 0.01, and ***p < 0.001, one-way ANOVA with Bonferroni post hoc test).

Tat-haFGF$_{14-154}$. Primary cortical neurons in vitro were used to confirm these results and explore the signaling pathway related to the upregulation of ADAM10 by Tat-haFGF$_{14-154}$. Inositol-requiring enzyme 1α (IRE1α), one of the three endoplasmic reticulum (ER) stress sensors, can active XBP1 by splicing XBP1u to XBP1s.[33] Phosphoinositide 3-kinase (PI3K) is one of the major signaling mediators of aFGF,[34] and its activation can be blocked by LY294002. Regulatory subunits p85α of PI3K promote the nuclear translocation of XBP1s.[35-37] cAMP response element-binding protein (CREB) is activated in AD models by PI3K/Akt, and its phosphorylation is neuroprotective.[38,39] CREB is also activated by ER stress, and it binds to the promoter of the IRE1α gene and regulates its expression.[40] Based on these findings, we hypothesized that Tat-haFGF$_{14-154}$ promotes the expression of ADAM10 through this PI3K-CREB-IRE1α/XBP1 pathway.

Levels of XBP1u, XBP1s, p-PI3K (p-p85α and Tyr467), PI3K (p85α), p-CREB (Ser133), and CREB were assayed by western blotting, and

the effects of PI3K inhibitor (LY294002) were assessed (Figures 7A–7E). After treatment with Tat-haFGF$_{14-154}$, XBP1s/XBP1u, phosphorylation of PI3K (p-PI3K/p-p85α and Tyr467), and phosphorylation of CREB (p-CREB and Ser133) were significantly increased in neurons injured by Aβ (p < 0.01), and they were suppressed by PI3K inhibitor (p < 0.001 in Figures 7C and 7D and p < 0.01 in Figure 7E). These results fueled our hypothesis that the PI3K-CREB-IRE1α/XBP1 pathway was activated by Tat-haFGF$_{14-154}$. PI3K inhibition abolished the rise in ADAM10 expression seen in neurons treated with T1500 + Aβ (p < 0.01 for P + T1500 + Aβ; Figures 7F and 7G) as well as thwarted haFGF$_{14-154}$ rescue of cell viability (p < 0.001 for P + T1500 + Aβ; Figure 7H) and morphological damage (Figure 7I).

DISCUSSION

AD has become a major public health problem owing to the increasing prevalence, long course of disease, burden on caregivers,
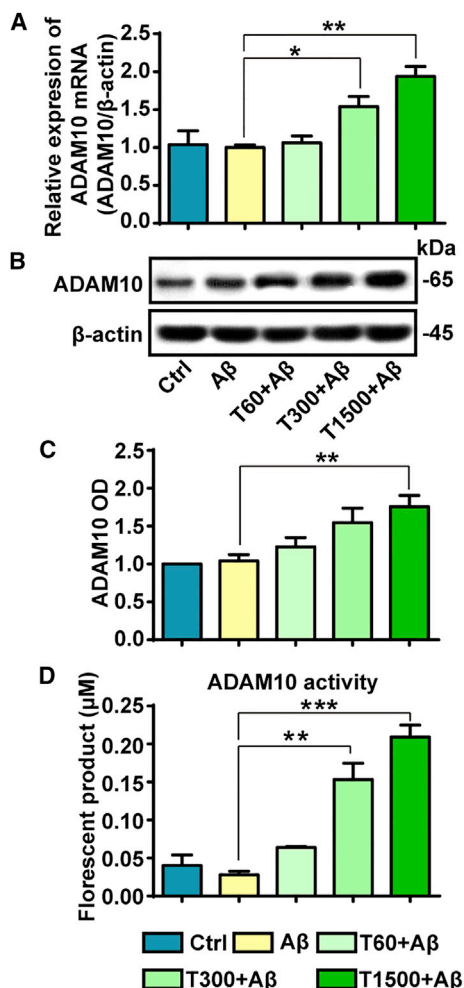
Figure 5. Tat-haFGF$_{14-154}$ Enhanced Expression and Activity of ADAM10 in Primary Neurons Injured by Aβ_{1-42}

Expressions of ADAM10 mRNA and protein levels were assayed by qRT-PCR and western blotting, respectively. (A) The expression of ADAM10 mRNA was normalized by β-actin. (B and C) Representative immunoblots (B) and quantification (C) of ADAM10 expression. (D) Activity of ADAM10. All values are presented as means ± SEM (n = 6; *p < 0.05, **p < 0.01, and ***p < 0.001, one-way ANOVA with Bonferroni post hoc test). OD, relative optical density.

and high financial cost of care.[41] New effective treatments that will prevent, delay, or treat the symptoms of AD are urgently needed. Neuroprotection of aFGF has been widely reported over the recent years,[15,42,43] yet its mechanism is still uncertain. In our study, Tat-haFGF$_{14-154}$-loaded cationic liposomes were delivered to APP/PS1 mice via intranasal administration to investigate neuroprotection of Tat-haFGF$_{14-154}$, and the related mechanism was explored in primary cortical neurons of rats injured by Aβ_{1-42}.

Tat-haFGF$_{14-154}$ Reverses Behavioral Deficits and Reduces Aβ Burden in APP/PS1 Mice

One of the great challenges for drugs targeting neurodegenerative diseases is that the BBB restricts the access of drugs to the brain by oral

and intravenous administration. Intranasal delivery has proven to be a new and noninvasive strategy, which can circumvent the BBB and facilitate direct transport of the drugs to the brain through neuronal and extracellular pathways.[44,45] Our previous studies showed that intranasal administration of TAT-haFGF could improve cognition and reduce Aβ deposits more significantly in APP/PS1 mice compared with intravenous injection.[18,21–23] In an animal model of Parkinson's disease induced by 6-OHDA, liposomes markedly assisted the delivery of basic fibroblast growth factor (bFGF) to the striatum and substantia nigra (SN), and they enhanced the neuroprotective effects of bFGF on dopaminergic neurons.[46] Liposomes also enhanced the levels of aFGF significantly in the EC, accompanied by amelioration in cognitive and non-cognitive behavioral deficits. Consistent with the behavioral improvement, Aβ burden was reduced in both the cortex and hippocampus of brain by intranasal treatment with Tat-haFGF$_{14-154}$-loaded cationic liposomes.

Aβ originates from proteolysis of APP by the sequential enzymatic actions of BACE1 and PS1, called APP amyloidogenic processing. Conversely, ADAM10 precludes Aβ generation by cleaving APP within the eventual Aβ sequence, called non-amyloidogenic processing.[3] There was a marked increase of ADAM10 in both expression and activity in the brains of mice with treatment of Tat-haFGF$_{14-154}$-loaded cationic liposomes. ADAM10-mediated non-β-amyloidosis processing via enhancing expression and activity of ADAM10 may be involved in the amelioration of behavioral deficits and the reduction of Aβ burden in APP/PS1 mice treated with Tat-haFGF$_{14-154}$.

ADAM10 Mediates Neuroprotection of Tat-haFGF$_{14-154}$ in AD Models

Recent reports have provided several candidate drugs or therapeutic methods to attenuate pathology in AD; most of them show its mechanism of modulating APP processing so as to alter APP toward non-amyloidogenic processing.[30,47–50] Overexpression of ADAM10 impressively reduced Aβ plaque load and soluble Aβ, and it additionally restored learning deficits in double-transgenic Alzheimer model mice.[6] ADAM10 is a metalloprotease with multiple functions in the brain. Besides the α-secretase in APP processing, ADAM10 also plays a critical role in regulating functional membrane proteins at the synapse.[7] Postnatal disruption of the ADAM10 in mouse brain caused epileptic seizures, learning deficits, altered spine morphology, and defective synaptic functions.[51] With the upregulation of ADAM10, Tat-haFGF$_{14-154}$ dose-dependently enhanced cell viability, and it reversed damage in soma and neurites of neurons damaged by Aβ. Tat-haFGF$_{14-154}$ increased synaptic proteins SYN and GAP43 significantly both in vitro and in vivo, indicating that Tat-haFGF$_{14-154}$ promoted nerve growth and possessed the potential of modulating synaptic plasticity.

After siRNA knockdown of ADAM10, damage in soma and neurites induced by Aβ could not be reversed by the Tat-haFGF$_{14-154}$ treatment with a decrease in cell viability, which suggested that ADAM10 is a key target for Tat-haFGF$_{14-154}$ to protect neurons
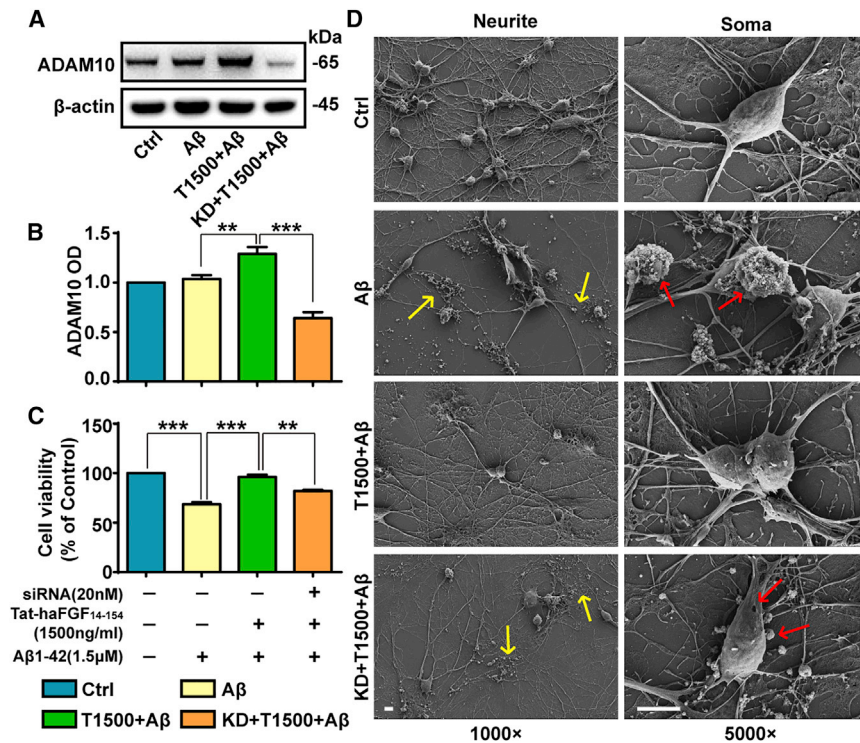
Figure 6. Knockdown of ADAM10 by siRNA Blocks Tat-haFGF$_{14-154}$ Neuroprotection

Neurons were treated with or without Aβ$_{1-42}$/Tat-haFGF$_{14-154}$/siRNA as described above. (A and B) Expression of ADAM10 in neurons was detected by western blotting. (C) Cell viability by MTT assay. (D) Morphological change of neurons was observed by scanning electronic microscope. The yellow arrows show fractured neurites or axons, and the red arrows show desiccated or damaged somas. All values are presented as means ± SEM (**p < 0.01 and ***p < 0.001, one-way ANOVA with Bonferroni post hoc test). KD, knockdown; OD, relative optical density.

from injury in the AD model. Pischedda and Piccoli[52] also reported that pharmacological inhibition of ADAM10 results in impairment of neurite outgrowth, and this modulation is involved in the FGFR2-signaling pathway. Recent progress in understanding the substrates and function as well as the regulation and cell biology of ADAM10 in the CNS highlights the value of ADAM10 as a drug target in brain diseases.[31]

Tat-haFGF$_{14-154}$ Upregulates ADAM10 via the PI3K-CREB-IRE1α/XBP1 Pathway

According to our results that Tat-haFGF$_{14-154}$ promoted mRNA expression of ADAM10, the upregulation of ADAM10 might happen at the transcriptional level. XBP1 efficiently upregulated ADAM10 expression; a reduced activity or presence of XBP1 could potentially be associated with an increased plaque burden and progression of AD.[32] PC12 cells overexpressing mXBP1s were fully protected at lethal doses of Aβ oligomers (18 mg/mL) and partially protected at higher concentrations of Aβ.[53] Endogenous XBP1 plays a critical role in preventing Aβ neurotoxicity, as shown by the exacerbated cell death induced by Aβ in AD models when XBP1 was eliminated.[53] IRE1α cleaves XBP1 pre-mRNA encoding for XBP1u in the cytoplasm, and this cytoplasmic splicing results in a new protein with transcriptional activity called XBP1s.[54] Mammalian IRE1α initiates diverse downstream signaling of the UPR either through splicing of XBP1 pre-mRNA to maintain cell survival or through posttranscriptional modifications via regulated IRE1-dependent decay (RIDD) of multiple substrates, which triggers cell apoptosis.[55,56] Tat-haFGF$_{14-154}$ enhanced the ratio of XBP1s/XBP1u in the brain

of APP/PS1 mice and primary neurons injured by Aβ, indicating that splicing XBP1 was activated by Tat-haFGF$_{14-154}$. Nuclear translocation of active XBP1s could be improved by the overexpression of PI3K regulatory subunits p85α,[37] and deletion of p85α showed a reduced accumulation of XBP1s in the nucleus,[57] revealing a link between PI3K and the IRE1α/XBP1 pathway. The PI3K pathway is one of the most important intracellular signaling cascades induced by aFGF too.[34] Phosphorylation of PI3K was upregulated by Tat-haFGF$_{14-154}$ in primary neurons damaged by Aβ, but no change of PI3K expression was found. It meant that Tat-haFGF$_{14-154}$ activated the PI3K pathway but didn't influence the translocation of XBP1s.

CREB is critically involved in the regulation of synaptic plasticity, intrinsic excitability, and long-term memory formation.[58] Its activation exhibits neuroprotection via the PI3K/Akt/CREB pathway in AD models.[38,39] CREB is also activated by ER stress: a chromatin immunoprecipitation assay indicated that CREB binds to the promoter region of IRE1α genes and regulates its expression.[40] Expression of IRE1α was increased concomitantly with CREB phosphorylation in human glioma cells treated with nitric oxide (NO).[59] Phosphorylation of CREB was upregulated by Tat-haFGF$_{14-154}$, and no change of CREB expression was found in primary neurons injured by Aβ. The activation of the CREB pathway and the splicing of XBP1 induced by Tat-haFGF$_{14-154}$ were blocked by PI3K inhibitor, resulting in a disappearing rescue of cell viability and morphological damage. These results suggest that the activation of the PI3K pathway is related to the activation of CREB and the downstream splicing of XBP1 induced by IRE1α.

In conclusion, Tat-haFGF$_{14-154}$ treatment significantly ameliorated the behavioral deficits of APP/PS1 mice, relieved Aβ burden, and increased the expression and activity of ADAM10 in the brain. Tat-haFGF$_{14-154}$ antagonized Aβ$_{1-42}$-induced cell death and structure damage in primary neurons in an ADAM10-dependent manner following the activation of XBP1 splicing and the PI3K-CREB pathway. As shown in Figure 8, Tat-haFGF$_{14-154}$ binds to its receptor,
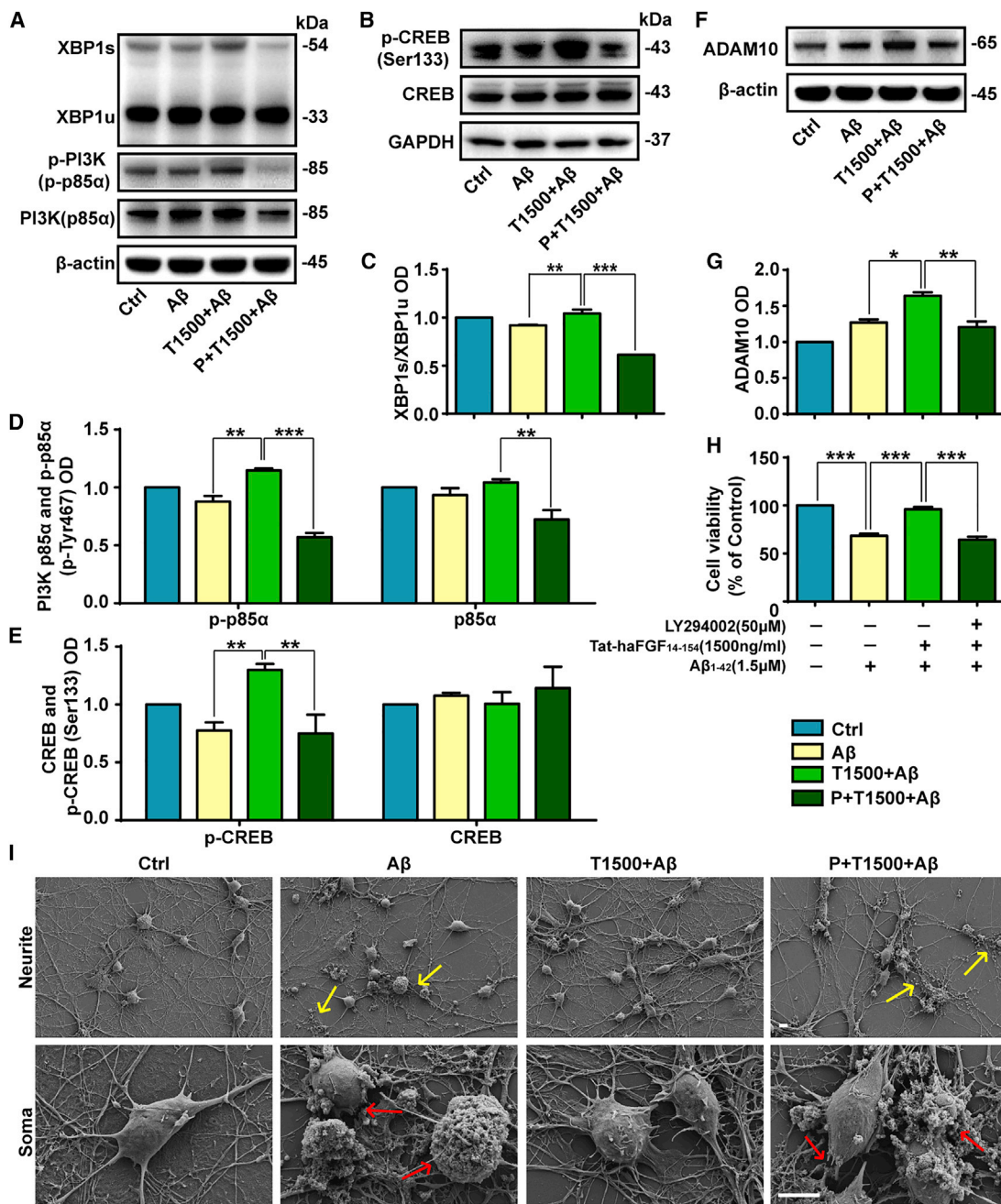
Figure 7. Tat-haFGF$_{14-154}$ Upregulated the Expression of ADAM10 via the PI3K-CREB-IRE1α/XBP1 Pathway

Primary neurons were pre-treated for 30 min with PI3K inhibitor (LY294002, P), followed by incubation with Tat-haFGF$_{14-154}$ and Aβ$_{1-42}$ as described above. (A and B) Representative immunoblots of XBP1s, XBP1u, p-PI3K(p-p85α and Tyr467), PI3K(p85α), p-CREB (Ser133), and CREB. (C–E) Quantitative analysis for XBP1s/XBP1u (C), expression of PI3K p85α and p-p85α (D), and p-CREB (Ser133) and CREB (E). (F and G) Upregulation of ADAM10 induced by Tat-haFGF$_{14-154}$ was blocked by the PI3K inhibitor. (H) Cell viability was decreased by PI3K inhibitor. (I) The PI3K inhibitor subverted the improvement effect of Tat-haFGF$_{14-154}$ on cell morphology. The yellow arrows show fractured neurites or axons, and the red arrows show desiccated or damaged somas. All values are presented as means ± SEM (n = 6; *$p < 0.05$, **$p < 0.01$, and ***$p < 0.001$, one-way ANOVA with Bonferroni post hoc test for C, G, and H, two-way ANOVA with Bonferroni's post hoc test for D and E). P, PI3K inhibitor LY294002; XBP1s, spliced XBP1 protein; XBP1u, unspliced XBP1protein; OD, relative optical density.
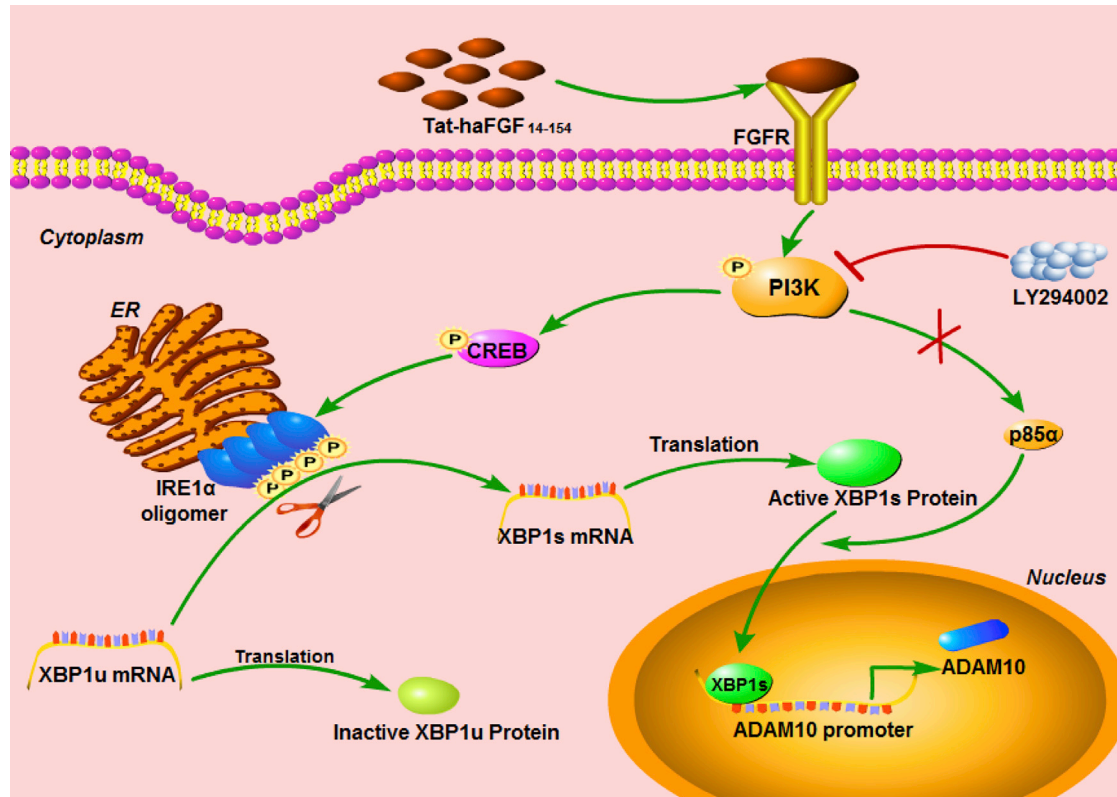
Figure 8. Signaling Pathway for Tat-haFGF$_{14-154}$ Neuroprotection

Tat-haFGF$_{14-154}$ binds to its receptor, activating the PI3K pathway, leading to CREB activation followed by the splicing of XBP1u mRNA to XBP1s mRNA in the ER. The XBP1s mRNA generated is translated to active XBP1s protein, a transcription factor for ADAM10.[32] The nuclear translocation of active XBP1s can be promoted by the PI3K regulatory subunit p85α,[35–37] but Tat-haFGF$_{14-154}$ does not alter the level of p85α. LY294002 inhibits the phosphorylation of PI3K and the splicing of XBP1, inhibiting the expression of ADAM10.

activating the PI3K pathway, leading to CREB activation followed by the splicing of XBP1u mRNA to XBP1s mRNA in the ER. The XBP1s mRNA generated is translated to active XBP1s protein, a transcription factor for ADAM10.[32] These results highlight the important role of ADAM10 as a key target in neuroprotection of Tat-haFGF$_{14-154}$, suggesting that Tat-haFGF$_{14-154}$ has the potential to be an alternative therapy to attenuate the AD pathological process.

MATERIALS AND METHODS

Preparation of Tat-haFGF$_{14-154}$-Loaded Cationic Liposomes

Recombinant fusion protein Tat-haFGF$_{14-154}$ was expressed and purified from our lab as reported previously.[14,18] Liposomes were produced by the method of pH gradient.[60] Tat-haFGF$_{14-154}$ was incubated with liposomes in different ratios (1:100, 1:50, 1:10, 1:5, 1:2, and 4:5) for 30 min at 25°C or 30°C. Encapsulation efficiency of cationic liposomes was calculated by a formula: Encapsulation efficiency (Q) % = $(C_{total} - C_{free})/C_{total} \times 100$. Free Tat-haFGF$_{14-154}$ (C_{free}) and total Tat-haFGF$_{14-154}$ (C_{total}) were separated by microcolumn centrifugation method. The content of Tat-haFGF$_{14-154}$-loaded cationic liposomes was assayed by human FGF acidic ELISA Kit (R&D Systems), according to the manufacturer's instructions.

Coomassie blue staining was applied after electrophoresis with 12% SDS-PAGE to detect SDS-resistant polymerization of Tat-haFGF$_{14-154}$ after 0, 0.5, or 1 hr incubation with cationic liposomes.

Animals and Treatment

APPswe/PS1d9 double-transgenic mice (APP/PS1) and wild-type background-matched mice (7 months old) were purchased from Beijing HuaFuKang Biotechnology. Mice were kept under conditions of controlled temperature (24°C ± 1°C), humidity (~50%–60%), and a light/dark cycle of 12/12 hr (light on at 8:00 a.m.). Mice were free to access standard rodent diet and water. Aliquots of 0.9% saline (vehicle), 600 μg/kg Tat-haFGF$_{14-154}$ (T600), and 600 μg/kg Tat-haFGF$_{14-154}$-loaded cationic liposomes (L + T600) were intranasally administered as a single dose to wild-type mice, which were then sacrificed in after 30 min. Distribution of aFGF in OB and EC was detected by western blotting. APP/PS1 mice were treated with the same doses of the same agents by intranasal delivery every 2 days for 6 weeks according to the modified method of *Capsoni*.[61] All experiments were conducted according to the guidelines for animal care and use of China, and they were approved by the animal ethics committee of the Chinese Academy of Medical Science.

MWM

After treatment for 5 weeks, learning and memory abilities of mice were assayed by MWM.[62] The maze consisted of a steel pool (120-cm diameter) filled with opaque water at $22°C \pm 1°C$ and a steel platform (10 cm^2). An overhead video camera connected to Ethovsion XT (Noldus Information Technology) was used to track the movement of mice and record all trials. In the place navigation test, the hidden platform (1 cm under water level) was kept constant in the middle of one quadrant throughout training. The training consisted of 6-day trials (one trial per quadrant and four quadrants per day, with a 20-min interval between each trial). Records were taken from the first day (day 0) of the training. Training on day 0 ensured the mice adapted to the swimming environment. Each trial lasted until the mouse climbed onto the hidden platform target within 60 s, and the escape latency onto the platform and the path length were recorded. The spatial probe test without the platform was conducted 24 hr after completing the last training trial (day 5). Each mouse was put into the pool for 60 s from the most distant to the target quadrant, and the percentage of time spent on each quadrant and times of crossing the removed-platform area were measured.

NC and OF Tests

NC and OF tests were conducted 24 hr after completing the MWM test. Mice were transferred to individual cages with bedding but no environmental enrichment items 1 hr before the dark phase commenced. The mouse was given access to a piece of cotton gauze (~5-cm squares, weighing 3 g) in each cage. The next morning the nesting score of each mouse was calculated according to a standard five-point nest-rating scale.[63]

An OF chamber was used to assess motor activity and anxiety-like behavior. The chamber was a brightly and evenly illuminated square area (50 × 50 × 25 cm) made of white glacial polyvinyl chloride and illuminated with four 60-W lamps (mounted 1.5 m above). The area was divided into 16 quadrants (four central and 12 peripheral).[64] Mice were placed individually in the center of the OF, left to explore for 5 min, and videotaped under white illumination. Time spent in the center, number of crossings through the central area, and total distance movement were recorded and analyzed by Ethovision XT (Noldus Information Technology).

Immunohistochemical Detection

The right hemisphere of APP/PS1 mice was fixed in 4% paraformaldehyde (Guoyao) and embedded with paraffin. Coronal paraffin sections (6-μm thick) were dewaxed, rehydrated, and treated with 3% H_2O_2/methanol solution for 10 min. Then, sections were boiled for 15 min in 0.01 M citrate buffer (pH 6.0). After the citrate buffer returned to room temperature, sections were washed with PBS and incubated in blocking solution (5% BSA) for 1 hr at 37°C, followed by being incubated overnight with primary antibodies at 4°C in a humidified chamber. Primary antibodies included anti-synaptophysin (1:250, Abcam) and anti-GAP43 (1:250, Abcam) rabbit antibodies and mouse monoclonal anti-Aβ antibody (6E10, 1:500, Covance). After being washed with PBS, the sections were incubated with

anti-mouse or rabbit IgG-horseradish peroxidase (HRP) secondary antibody for 1 hr at 37°C, followed by diaminobenzidine (DAB) (Boster Biotech) and hematoxylin staining. Slides were assessed by light microscope (IX71, Olympus) and micrographs were analyzed by Image-Pro plus 6.0 software.

Western Blotting

Tissue homogenates and cultured cells were lysed in radioimmunoprecipitation assay (RIPA) lysis buffer (Beyotime) with PMSF (Sigma-Aldrich) and Protease Inhibitor Cocktail (Roche) on ice. Lysates in supernatant were separated by centrifuging at 13,000 rpm at 4°C for 15 min. The concentration of total protein was measured by BCA Protein Assay Kit (Thermo Fisher Scientific). Samples were electrophoresed in NuPAGE 4%–12% Bis-Tris Gels (Thermo Fisher Scientific) with NuPAGE MES SDS Running Buffer (Thermo Fisher Scientific), and they were electrophoretically transferred to polyvinylidene difluoride (PVDF) membranes (Millipore). After being dipped in 0.2% glutaraldehyde (Sigma-Aldrich) for 30 min, membranes were blocked for ~1–2 hr at room temperature and then incubated at 4°C overnight with the following primary antibodies: mouse aFGF monoclonal antibody (1:1,000, Sigma), rabbit anti-synaptopysin antibody (1:1,000, Abcam), rabbit anti-GAP43 antibody (1:1,000, Abcam), 6E10 mouse monoclonal antibody (1:2,000, Covance), ADAM10 rabbit monoclonal antibody, BACE1 rabbit monoclonal antibody, PS1 rabbit monoclonal antibody (1:1,000, Abcam), anti-APP(C-terminal) rabbit monoclonal antibody (1:4,000, Sigma), phospho-PI3k p85á/p55á (Tyr 467/Tyr 199) rabbit antibody, PI3 kinase p85á/p55á rabbit monoclonal antibody (1:1,000, Bioworld), β-actin rabbit monoclonal antibody (1:1,000, Cell Signaling Technology), XBP-1 rabbit polyclonal antibody (1:1,000, Abcam), CREB rabbit monoclonal antibody (1:1,000, Cell Signaling Technology), phospho-CREB (Ser 133) rabbit monoclonal antibody (1:1,000, Cell Signaling Technology), and GAPDH rabbit monoclonal antibody (1:1,000, Cell Signaling Technology). After incubation with secondary antibody (peroxidase-conjugated affinipure goat anti-rabbit/mouse IgG, 1:2,000, Proteintech) for 2 hr at room temperature, the blots were detected with SuperSignal West Pico chemiluminescent substrate (Pierce Biotechnology).

Enzyme Activity Assay

Activities of ADAM10 and BACE1 were measured by SensoLyte 520 ADAM10 Activity Assay Kit (Anaspec) and β-secretase (BACE1) Activity Detection Kit (Sigma-Aldrich), according to the manufacturers' instructions.

Cell Culture and Treatments

Primary cortical neurons were separated from brains of newborn Sprague-Dawley (SD) rats. Tissues were cut rapidly into small pieces in D-Hank's buffer, then digested with 0.25% trypsin for 10 min at 37°C. DMEM (high glucose, Thermo Fisher Scientific) containing 10% fetal bovine serum (FBS) (Thermo Fisher Scientific) was then added. The cell suspension was filtered, then centrifuged at 250 × g for 5 min. Cells were cultured in Neurobasal-A Medium (Thermo Fisher Scientific) supplemented with 2% B-27 supplement (50×,

serum free, Thermo Fisher Scientific) at 37°C. Small tissue mass and dead cells were removed by changing culture medium 4–6 hr after seeding. Neurons (5 DIV) were pre-treated with Tat-haFGF$_{14-154}$ (60, 300, and 1,500 ng/mL) for 2 hr at 37°C, and 1.5 μM Aβ$_{1-42}$ (Millipore) was added into the culture medium with continuous Tat-haFGF$_{14-154}$ treatment for 48 hr. Aβ$_{1-42}$ was dissolved in 0.1% DMSO and incubated in 37°C for 24 hr. In some cases, cells were treated with 50 nM PI3K inhibitor (LY294002, Cell Signaling Technology) 30 min before Tat-haFGF$_{14-154}$ treatment.

Cell Viability and Apoptosis Analysis

For viability analysis, cells were seeded in a 96-well culture plate at a density of 1×10^4 cells/well. After treatments, cells were incubated with 10 mL 5 mg/mL methyl thiazolyl tetrazolium (MTT) (Sigma) for 4 hr at 37°C. The supernatants were aspirated, and the formazan precipitates were solubilized by the addition of 100 μL DMSO per well. Absorbance at 570 nm was monitored by a Multiskan GO Spectrophotometer (Thermo Scientific).

For apoptosis analysis, cells were seeded in a six-well culture plate at a density of 1.5×10^6 cells/well. After treatments, cells were washed with PBS and fixed with 4% paraformaldehyde for 10 min at room temperature, then exposed to Hoechst 33342 (5 μg/mL) for 15 min at room temperature. Images were recorded by interactive laser cytometer (LSM 710 META, Carl Zeiss).

Scanning Electron Microscopy

Cells were seeded on 15-mm circular glass coverslips (NEST) in a 24-well culture plate. After treatments, samples were fixed with glutaraldehyde (Sigma-Aldrich) overnight at 4°C, followed by being rinsed and dehydrated in an alcohol gradient (30%, 50%, 70%, and 90% for 3 min each and 100% for 15 min). Cells on the coverslips were incubated with isoamyl acetate (Dongzheng) for 5 min twice, dried by a critical point dryer (Emitech K850X, Quorum), followed by gold-palladium sputtering. The coverslips were fixed on specimen mount with conductive adhesive, and the cell surfaces were examined by scanning electron microscope (Carl Zeiss).

Immunofluorescence

To detect the location and expression of synaptic proteins, primary cortical neurons were seeded in 35-mm confocal dishes (Corning) at a density of 1.5×10^6 cells/well. After treatments, cells were fixed with 4% paraformaldehyde (PFA) for 15 min and permeabilized with 0.1% Triton X-100 (Sigma) for 20 min at room temperature, followed by incubation with blocking buffer (Beyotime) for 1 hr at room temperature. Then, samples were incubated with primary antibodies overnight at 4°C, including rabbit anti-GAP43 antibody (1:250, Abcam) and rabbit anti-synaptopysin antibody (1:250, Abcam). After being washed with PBS, cells were incubated with anti-rabbit IgG-H&L secondary antibody (DyLight 488, 1:200, Abcam) for 1 hr at 37°C and kept in the dark, followed by DAPI nuclear staining (0.5 μg/mL, Beyotime) for 15 min. Images of cells were recorded by interactive laser cytometer (LSM 710 META, Carl Zeiss), and micrographs were analyzed using Image-Pro plus 6.0 software.

RNA Isolation and qRT-PCR Assay

Total RNA of cultured cells was extracted with HiPure Total RNA Mini Kit (Magen) and quantified by Nanodrop 2000 (Thermo Fisher Scientific). The iScript cDNA Synthesis Kit (Bio-Rad) was used to synthesize the first-strand cDNA. The qPCR was performed with SsoAdvanced Universal Supermixes (Bio-Rad) by CFX96 Connect Real-Time PCR Detection System (Bio-Rad). Sequences of ADAM10 primers were ACAGACTTGGCTCTCGATAAACTT (forward) and GGTATGTACATTGGCAAGTGATGT (reverse). β-actin was used as an internal control and its primers were CCCGCGAGTACAACCTTCTTG (forward) and TCATCCATGG CGAACTGGTGG (reverse).

siRNA Transfection

The siRNA duplexes against ADAM10 were designed by us and synthesized by Genepharma with the following sequences: CCAGCA GAGAGAUAUAUUATT (sense) and UAAUAUAUCUCUCUGCU GGTT (anti-sense). Scrambled-siRNA sequences were UUCUCCGA ACGUGUCACGUTT (sense) and ACGUGACACGUUCGGAGA ATT (anti-sense). Primary cortical neurons were seeded on six-well plates at a density of 1.5×10^6 cells/well. Cells (5 DIV) were transfected with 20 nM scrambled-siRNA or targeted-siRNA using Lipofectamine RNAiMAX Reagent (Invitrogen). The knockdown efficiency was validated by qRT-PCR and western blot after siRNAs were transfected for 48 or 72 hr.

Statistical Analysis

One-way ANOVA followed by Bonferroni post hoc test or two-way ANOVA followed by Bonferroni multiple comparison tests was used for data analyses with statistics software (SPSS 19.0). All experimental data represent means ± SEM, and $p < 0.05$ was considered statistically significant.

SUPPLEMENTAL INFORMATION

Supplemental Information includes seven figures and can be found with this article online at http://dx.doi.org/10.1016/j.omtn.2017.05.004.

AUTHOR CONTRIBUTIONS

CONFLICTS OF INTEREST

The authors declare no conflicts of interest.

ACKNOWLEDGMENTS

REFERENCES

1. Maeda, J., Zhang, M.R., Okauchi, T., Ji, B., Ono, M., Hattori, S., Kumata, K., Iwata, N., Saido, T.C., Trojanowski, J.Q., et al. (2011). In vivo positron emission tomographic imaging of glial responses to amyloid-beta and tau pathologies in mouse models of Alzheimer's disease and related disorders. J. Neurosci. 31, 4720–4730.

2. Lesné, S.E., Sherman, M.A., Grant, M., Kuskowski, M., Schneider, J.A., Bennett, D.A., and Ashe, K.H. (2013). Brain amyloid-β oligomers in ageing and Alzheimer's disease. Brain 136, 1383–1398.

3. Haass, C., and Selkoe, D.J. (2007). Soluble protein oligomers in neurodegeneration: lessons from the Alzheimer's amyloid beta-peptide. Nat. Rev. Mol. Cell Biol. 8, 101–112.

4. Corbett, G.T., Gonzalez, F.J., and Pahan, K. (2015). Activation of peroxisome proliferator-activated receptor α stimulates ADAM10-mediated proteolysis of APP. Proc. Natl. Acad. Sci. USA 112, 8445–8450.

5. Obregon, D., Hou, H., Deng, J., Giunta, B., Tian, J., Darlington, D., Shahaduzzaman, M., Zhu, Y., Mori, T., Mattson, M.P., and Tan, J. (2012). Soluble amyloid precursor protein-α modulates β-secretase activity and amyloid-β generation. Nat. Commun. 3, 777.

6. Postina, R., Schroeder, A., Dewachter, I., Bohl, J., Schmitt, U., Kojro, E., Prinzen, C., Endres, K., Hiemke, C., Blessing, M., et al. (2004). A disintegrin-metalloproteinase prevents amyloid plaque formation and hippocampal defects in an Alzheimer disease mouse model. J. Clin. Invest. 113, 1456–1464.

7. Marcello, E., Saraceno, C., Musardo, S., Vara, H., de la Fuente, A.G., Pelucchi, S., Di Marino, D., Borroni, B., Tramontano, A., Pérez-Otaño, I., et al. (2013). Endocytosis of synaptic ADAM10 in neuronal plasticity and Alzheimer's disease. J. Clin. Invest. 123, 2523–2538.

8. Tuszynski, M.H., Thal, L., Pay, M., Salmon, D.P., U, H.S., Bakay, R., Patel, P., Blesch, A., Vahlsing, H.L., Ho, G., et al. (2005). A phase 1 clinical trial of nerve growth factor gene therapy for Alzheimer disease. Nat. Med. 11, 551–555.

9. Nagahara, A.H., Merrill, D.A., Coppola, G., Tsukada, S., Schroeder, B.E., Shaked, G.M., Wang, L., Blesch, A., Kim, A., Conner, J.M., et al. (2009). Neuroprotective effects of brain-derived neurotrophic factor in rodent and primate models of Alzheimer's disease. Nat. Med. 15, 331–337.

10. Cuevas, P., and Giménez-Gallego, G. (1996). Antiepileptic effects of acidic fibroblast growth factor examined in kainic acid-mediated seizures in the rat. Neurosci. Lett. 203, 66–68.

11. Jankowsky, J.L., and Patterson, P.H. (2001). The role of cytokines and growth factors in seizures and their sequelae. Prog. Neurobiol. 63, 125–149.

12. Reuss, B., and von Bohlen und Halbach, O. (2003). Fibroblast growth factors and their receptors in the central nervous system. Cell Tissue Res. 313, 139–157.

13. Xu, H., Li, X.K., Zheng, Q., Huang, Y.D., Yao, C.C., Su, Z.J., Zhao, W., and Zhao, Z.Y. (2009). Protective effects of mutant of acidic fibroblast growth factor against cerebral ischaemia-reperfusion injury in rats. Injury 40, 963–967.

14. Wang, Y., Lin, H., Lin, S., Qu, J., Xiao, J., Huang, Y., Xiao, Y., Fu, X., Yang, Y., and Li, X. (2010). Cell-penetrating peptide TAT-mediated delivery of acidic FGF to retina and protection against ischemia-reperfusion injury in rats. J. Cell. Mol. Med. 14, 1998–2005.

15. Wu, J.C., Huang, W.C., Tsai, Y.A., Chen, Y.C., and Cheng, H. (2008). Nerve repair using acidic fibroblast growth factor in human cervical spinal cord injury: a preliminary Phase I clinical study. J. Neurosurg. Spine 8, 208–214.

16. Wu, J.C., Huang, W.C., Chen, Y.C., Tu, T.H., Tsai, Y.A., Huang, S.F., Huang, H.C., and Cheng, H. (2011). Acidic fibroblast growth factor for repair of human spinal cord injury: a clinical trial. J. Neurosurg. Spine 15, 216–227.

17. Mashayekhi, F., Hadavi, M., Vaziri, H.R., and Naji, M. (2010). Increased acidic fibroblast growth factor concentrations in the serum and cerebrospinal fluid of patients with Alzheimer's disease. J. Clin. Neurosci. 17, 357–359.

18. Huang, Y., Rao, Y., Feng, C., Li, Y., Wu, X., Su, Z., Xiao, J., Xiao, Y., Feng, W., and Li, X. (2008). High-level expression and purification of Tat-haFGF19-154. Appl. Microbiol. Biotechnol. 77, 1015–1022.

19. Illum, L. (2002). Nasal drug delivery: new developments and strategies. Drug Discov. Today 7, 1184–1189.

20. Dhuria, S.V., Hanson, L.R., and Frey, W.H., 2nd (2010). Intranasal delivery to the central nervous system: mechanisms and experimental considerations. J. Pharm. Sci. 99, 1654–1673.

21. Xu, J., Xiang, Q., Su, J., Yang, P., Zhang, Q., Su, Z., Xiao, F., and Huang, Y. (2014). Evaluation of the safety and brain-related tissues distribution characteristics of TAT-HaFGF via intranasal administration. Biol. Pharm. Bull. 37, 1149–1157.

22. Lou, G., Zhang, Q., Xiao, F., Xiang, Q., Su, Z., Zhang, L., Yang, P., Yang, Y., Zheng, Q., and Huang, Y. (2012). Intranasal administration of TAT-haFGF$_{(14-154)}$ attenuates disease progression in a mouse model of Alzheimer's disease. Neuroscience 223, 225–237.

23. Lou, G., Zhang, Q., Xiao, F., Xiang, Q., Su, Z., and Huang, Y. (2016). Intranasal TAT-haFGF Improves Cognition and Amyloid-β Pathology in an AβPP/PS1 Mouse Model of Alzheimer's Disease. J. Alzheimers Dis. 51, 985–990.

24. Lai, F., Fadda, A.M., and Sinico, C. (2013). Liposomes for brain delivery. Expert Opin. Drug Deliv. 10, 1003–1022.

25. Samad, A., Sultana, Y., and Aqil, M. (2007). Liposomal drug delivery systems: an update review. Curr. Drug Deliv. 4, 297–305.

26. Schnyder, A., and Huwyler, J. (2005). Drug transport to brain with targeted liposomes. NeuroRx 2, 99–107.

27. Filali, M., and Lalonde, R. (2009). Age-related cognitive decline and nesting behavior in an APPswe/PS1 bigenic model of Alzheimer's disease. Brain Res. 1292, 93–99.

28. Arendash, G.W., King, D.L., Gordon, M.N., Morgan, D., Hatcher, J.M., Hope, C.E., and Diamond, D.M. (2001). Progressive, age-related behavioral impairments in transgenic mice carrying both mutant amyloid precursor protein and presenilin-1 transgenes. Brain Res. 891, 42–53.

29. Biallosterski, B.T., Prickaerts, J., Rahnama'i, M.S., de Wachter, S., van Koeveringe, G.A., and Meriaux, C. (2015). Changes in voiding behavior in a mouse model of Alzheimer's disease. Front. Aging Neurosci. 7, 160.

30. Zhang, Y.W., Thompson, R., Zhang, H., and Xu, H. (2011). APP processing in Alzheimer's disease. Mol. Brain 4, 3.

31. Saftig, P., and Lichtenthaler, S.F. (2015). The alpha secretase ADAM10: A metalloprotease with multiple functions in the brain. Prog. Neurobiol. 135, 1–20.

32. Reinhardt, S., Schuck, F., Grösgen, S., Riemenschneider, M., Hartmann, T., Postina, R., Grimm, M., and Endres, K. (2014). Unfolded protein response signaling by transcription factor XBP-1 regulates ADAM10 and is affected in Alzheimer's disease. FASEB J. 28, 978–997.

33. Cross, B.C., Bond, P.J., Sadowski, P.G., Jha, B.K., Zak, J., Goodman, J.M., Silverman, R.H., Neubert, T.A., Baxendale, I.R., Ron, D., and Harding, H.P. (2012). The molecular basis for selective inhibition of unconventional mRNA splicing by an IRE1-binding small molecule. Proc. Natl. Acad. Sci. USA 109, E869–E878.

34. Dailey, L., Ambrosetti, D., Mansukhani, A., and Basilico, C. (2005). Mechanisms underlying differential responses to FGF signaling. Cytokine Growth Factor Rev. 16, 233–247.

35. Park, S.W., Zhou, Y., Lee, J., Lu, A., Sun, C., Chung, J., Ueki, K., and Ozcan, U. (2010). The regulatory subunits of PI3K, p85alpha and p85beta, interact with XBP-1 and increase its nuclear translocation. Nat. Med. 16, 429–437.

36. Winnay, J.N., Boucher, J., Mori, M.A., Ueki, K., and Kahn, C.R. (2010). A regulatory subunit of phosphoinositide 3-kinase increases the nuclear accumulation of X-box-binding protein-1 to modulate the unfolded protein response. Nat. Med. 16, 438–445.

37. Winnay, J.N., and Kahn, C.R. (2011). PI 3-kinase regulatory subunits as regulators of the unfolded protein response. Methods Enzymol. 490, 147–158.

38. Jeon, S., Park, J.E., Lee, J., Liu, Q.F., Jeong, H.J., Pak, S.C., Yi, S., Kim, M.H., Kim, C.W., Park, J.K., et al. (2015). Illite improves memory impairment and reduces Aβ level in the Tg-APPswe/PS1dE9 mouse model of Alzheimer's disease through Akt/CREB and GSK-3β phosphorylation in the brain. J. Ethnopharmacol. 160, 69–77.

39. Singh, A.K., Kashyap, M.P., Tripathi, V.K., Singh, S., Garg, G., and Rizvi, S.I. (2016). Neuroprotection Through Rapamycin-Induced Activation of Autophagy and PI3K/Akt1/mTOR/CREB Signaling Against Amyloid-β-Induced Oxidative Stress, Synaptic/Neurotransmission Dysfunction, and Neurodegeneration in Adult Rats. Mol. Neurobiol. 1–14.

40. Kikuchi, D., Tanimoto, K., and Nakayama, K. (2016). CREB is activated by ER stress and modulates the unfolded protein response by regulating the expression of IRE1α and PERK. Biochem. Biophys. Res. Commun. 469, 243–250.

41. Li, J., Wu, H.M., Zhou, R.L., Liu, G.J., and Dong, B.R. (2008). Huperzine A for Alzheimer's disease. Cochrane Database Syst. Rev. (2), CD005592.

42. Tsai, M.J., Tsai, S.K., Huang, M.C., Liou, D.Y., Huang, S.L., Hsieh, W.H., Huang, W.C., Huang, S.S., and Cheng, H. (2015). Acidic FGF promotes neurite outgrowth of cortical neurons and improves neuroprotective effect in a cerebral ischemic rat model. Neuroscience 305, 238–247.

43. Thorns, V., and Masliah, E. (1999). Evidence for neuroprotective effects of acidic fibroblast growth factor in Alzheimer disease. J. Neuropathol. Exp. Neurol. 58, 296–306.

44. Alam, M.I., Beg, S., Samad, A., Baboota, S., Kohli, K., Ali, J., Ahuja, A., and Akbar, M. (2010). Strategy for effective brain drug delivery. Eur. J. Pharm. Sci. 40, 385–403.

45. Illum, L. (2000). Transport of drugs from the nasal cavity to the central nervous system. Eur. J. Pharm. Sci. 11, 1–18.

46. Yang, P.H., Zhu, J.X., Huang, Y.D., Zhang, X.Y., Lei, P., Bush, A.I., Xiang, Q., Su, Z.J., and Zhang, Q.H. (2016). Human Basic Fibroblast Growth Factor Inhibits Tau Phosphorylation via the PI3K/Akt-GSK3β Signaling Pathway in a 6-Hydroxydopamine-Induced Model of Parkinson's Disease. Neurodegener. Dis. 16, 357–369.

47. Branca, C., Sarnico, I., Ruotolo, R., Lanzillotta, A., Viscomi, A.R., Benarese, M., Porrini, V., Lorenzini, L., Calzà, L., Imbimbo, B.P., et al. (2014). Pharmacological targeting of the β-amyloid precursor protein intracellular domain. Sci. Rep. 4, 4618.

48. Li, B., Yu, D., and Xu, Z. (2014). Activated protein C inhibits amyloid β production via promoting expression of ADAM-10. Brain Res. 1545, 35–44.

49. Zhang, S.Q., Sawmiller, D., Li, S., Rezai-Zadeh, K., Hou, H., Zhou, S., Shytle, D., Giunta, B., Fernandez, F., Mori, T., and Tan, J. (2013). Octyl gallate markedly promotes anti-amyloidogenic processing of APP through estrogen receptor-mediated ADAM10 activation. PLoS ONE 8, e71913.

50. Zhang, Y., Yin, F., Liu, J., Liu, Z., Guo, L., Xia, Z., and Zidichouski, J. (2015). Geniposide attenuates insulin-deficiency-induced acceleration of β-amyloidosis in an APP/PS1 transgenic model of Alzheimer's disease. Neurochem. Int. 89, 7–16.

51. Prox, J., Bernreuther, C., Altmeppen, H., Grendel, J., Glatzel, M., D'Hooge, R., Stroobants, S., Ahmed, T., Balschun, D., Willem, M., et al. (2013). Postnatal disruption of the disintegrin/metalloproteinase ADAM10 in brain causes epileptic seizures, learning deficits, altered spine morphology, and defective synaptic functions. J. Neurosci. 33, 12915–12928.

52. Pischedda, F., and Piccoli, G. (2016). The IgLON Family Member Negr1 Promotes Neuronal Arborization Acting as Soluble Factor via FGFR2. Front. Mol. Neurosci. 8, 89.

53. Casas-Tinto, S., Zhang, Y., Sanchez-Garcia, J., Gomez-Velazquez, M., Rincon-Limas, D.E., and Fernandez-Funez, P. (2011). The ER stress factor XBP1s prevents amyloid-beta neurotoxicity. Hum. Mol. Genet. 20, 2144–2160.

54. Yoshida, H., Matsui, T., Yamamoto, A., Okada, T., and Mori, K. (2001). XBP1 mRNA is induced by ATF6 and spliced by IRE1 in response to ER stress to produce a highly active transcription factor. Cell 107, 881–891.

55. Chen, Y., and Brandizzi, F. (2013). IRE1: ER stress sensor and cell fate executor. Trends Cell Biol. 23, 547–555.

56. Han, D., Lerner, A.G., Vande Walle, L., Upton, J.P., Xu, W., Hagen, A., Backes, B.J., Oakes, S.A., and Papa, F.R. (2009). IRE1alpha kinase activation modes control alternate endoribonuclease outputs to determine divergent cell fates. Cell 138, 562–575.

57. Winnay, J.N., Boucher, J., Mori, M., Ueki, K., and Kahn, C.R. (2010). A Novel Interaction Between the Regulatory Subunit of PI 3-Kinase and X-box Binding Protein-1 Modulates the Unfolded Protein Response. Nat. Med. 16, 438–445.

58. Barco, A., and Marie, H. (2011). Genetic approaches to investigate the role of CREB in neuronal plasticity and memory. Mol. Neurobiol. 44, 330–349.

59. Kim, Y.H., Joo, H.S., and Kim, D.S. (2010). Nitric oxide induction of IRE1-alpha-dependent CREB phosphorylation in human glioma cells. Nitric Oxide 23, 112–120.

60. Čeh, B., and Lasic, D.D. (1997). A Rigorous Theory of Remote Loading of Drugs into Liposomes: Transmembrane Potential and Induced pH-Gradient Loading and Leakage of Liposomes. J. Colloid Interface Sci. 185, 9–18.

61. Capsoni, S., Giannotta, S., and Cattaneo, A. (2002). Nerve growth factor and galantamine ameliorate early signs of neurodegeneration in anti-nerve growth factor mice. Proc. Natl. Acad. Sci. USA 99, 12432–12437.

62. Morris, R. (1984). Developments of a water-maze procedure for studying spatial learning in the rat. J. Neurosci. Methods 11, 47–60.

63. Deacon, R.M. (2006). Assessing nest building in mice. Nat. Protoc. 1, 1117–1119.

64. Fiore, L., and Ratti, G. (2007). Remote laboratory and animal behaviour: An interactive open field system. Comput. Educ. 49, 1299–1307.